Earth, Planets and Space

FULL PAPER Open Access

Identification of active faults and tectonic features through heat flow distribution in the Nankai Trough, Japan, based on high-resolution velocity-estimated bottom-simulating reflector depths

Shuto Takenouchi[1*], Takeshi Tsuji[1,2], Kazuya Shiraishi[3], Yasuyuki Nakamura[3], Shuichi Kodaira[3], Gou Fujie[3] and Kota Mukumoto[1]

Abstract

Estimates of heat flow can contribute to our understanding of geological structures in plate convergent zones that produce great earthquakes. We applied automated velocity analysis to obtain the accurate seismic profiles needed for precise heat flow estimates using six new seismic profiles acquired during R/V *Kaimei* KM18-10 voyage in 2018. We calculated heat flow values in the accretionary wedge of the Nankai Trough off the Kii Peninsula, Japan, from the positions of widespread bottom-simulating reflectors (BSRs) in seismic reflection profiles. Calculated conductive heat flow values from the depth of the BSR agree with previous studies where a regional trend is observed from ~ 50 mW/m^2 to < 40 mW/m^2 60 km landward from the deformation front. This trend is caused by thickening of accretionary sediments and the subduction of the Philippines Sea plate. Segments of profiles are marked by anomalous high heat flow values. Such anomalies represent alterations of the shallow crustal thermal structure caused either by a combination of topographic affects, surface erosion of the seafloor, or by fluid flow that transports heat by advection. We interpret heat flow anomalies (~ 100 mW/m^2) as indicators of active faulting, which correspond to low seismic velocity zones along faults. Our results also showed relatively high heat flow at the landward end of several survey lines close to the Kii Peninsula, which we interpret to the possible presence of plutonic rocks that underlie the Kii Peninsula and extend offshore and may be the cause of geothermal springs, steep geothermal gradients, and high heat flow.

Keywords Bottom-simulating reflector (BSR), Heat flow, Active faults, Plutonic rock, Seismic reflection data, Automated velocity analysis, P-wave velocity

*Correspondence:
Shuto Takenouchi
s.takenouchi@mine.kyushu-u.ac.jp; s.takenouchi0501@gmail.com
Full list of author information is available at the end of the article

Graphical abstract

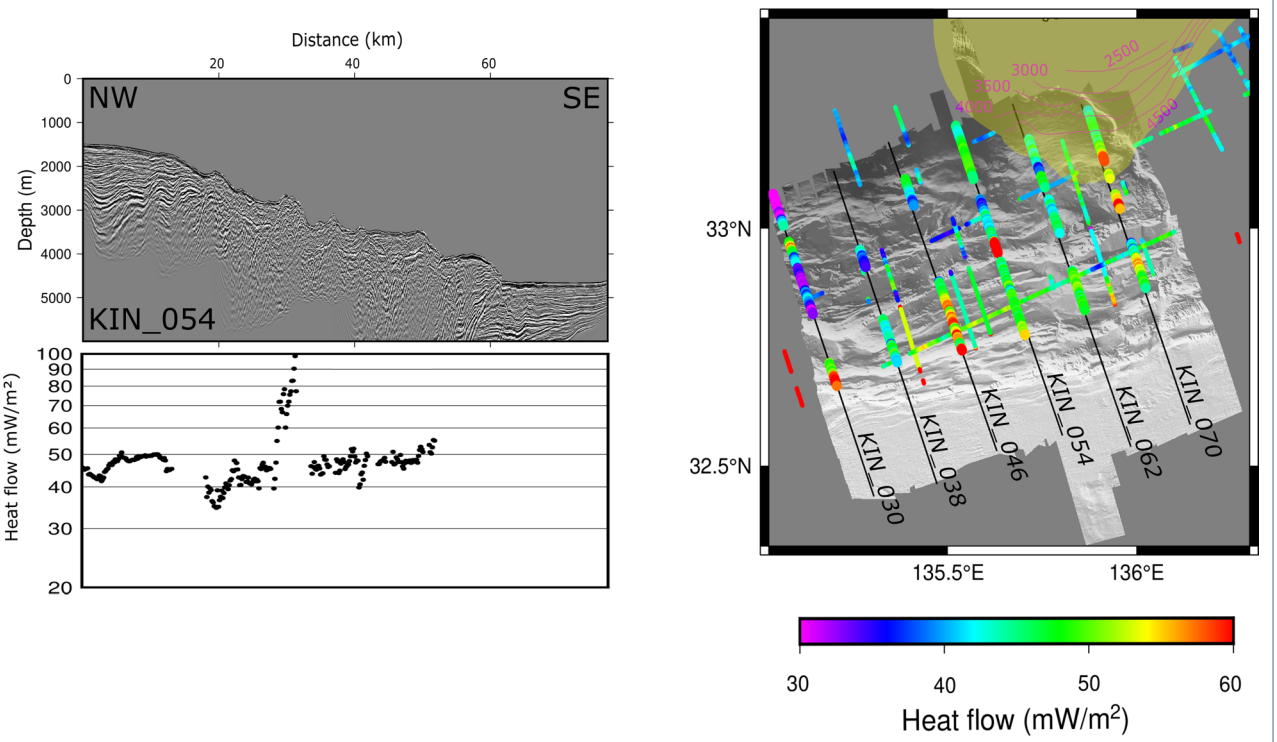

Introduction

Heat flow data are useful for interpreting geological features and process in subduction zones. Since heat flow can be affected by several different processes (e.g., the ascent of fluids toward the seafloor, rapid erosion and sedimentation, and tectonic uplift), we can infer aspects of tectonic activity or thermal regimes in subduction zones from heat flow data. Heat flow distribution has been investigated by several methods, including the use of seafloor sediment probes (Christoffel and Calhaem 1969), piston core samplers (Kinoshita et al. 2008), and the depth distribution of methane hydrate deposits derived from the position of bottom-simulating reflectors (BSRs) in seismic profiles (e.g., Yamano et al. 1982; Davis et al. 1990; Hyndman and Spence 1992).

BSRs, which mark the phase boundary between free methane gas below and methane hydrates above (Markl et al. 1970), appear in seismic profiles as high-amplitude reflectors with reverse polarity compared to the seafloor reflections and are nearly parallel to the seafloor (Vanneste et al. 2001). BSRs can be disrupted by several processes that also affect heat flow, allowing us to infer thermal conditions in the shallow sediments where BSRs appear.

In this study, we derived estimates of heat flow from the distribution of BSRs in the Nankai Trough and used this information to investigate geological features in the accretionary wedge. This method can provide continuously distributed heat flow data along seismic transects with finer resolution than direct in-situ measurement methods, which may help reveal geological structures. However, estimating heat flow from BSR profiles requires accurate depth information. In this study, we applied automated velocity analysis (Fomel et al. 2013) to obtain a high-resolution P-wave velocity structure (Mukumoto et al. 2019; Kret et al. 2020), which helped reveal the presence of free gas beneath the methane hydrate layer as low-velocity anomalies (Chhun et al. 2018; Eng and Tsuji 2019). Automated velocity analysis can incorporate all available seismic data to produce a seismic velocity model based on dense spatial coverage and hence yield seismic profiles with improved accuracy. In this paper, we describe our estimates of conductive heat flow derived from the improved depth model and discuss the geological structures inferred from the estimated heat flow anomalies.

The Nankai Trough is a well-studied plate subduction zone that has been investigated with a variety of

geophysical techniques including seismic, gravity, and electrical resistivity surveys (e.g., Honda and Kono 2005; Kasaya et al. 2005; Kodaira et al. 2007). Seismic reflection profiling is one of the most effective of these for characterizing the details of geological structures and physical properties. The detailed knowledge of heat flow derived from the high-resolution velocity and reflection profiles can help identify active faults that may affect thermal conditions. These inferred active faults could inform further geophysical surveys, for purposes such as optimal deployment of seismometer networks to monitor fluid flow and fault dynamics.

Geological setting

The Nankai Trough is a convergent plate boundary where the Philippine Sea plate is subducting beneath the Eurasian plate at approximately 3–5 cm/year (e.g., Seno et al. 1993). The Nankai Trough has been divided into several segments on the basis of the rupture zones of historical great earthquakes (e.g., Ando 1975; Cummins et al. 2002; Hori 2006), and one such segment is located off the Kii Peninsula. On the landward side of the trench, a sedimentary accretionary prism has formed on the Eurasian plate, overlain by a forearc basin. The imbricate thrust zone (ITZ), in the middle of the accretionary prism, is defined as weak folding and inclined turbidite beds consisting of fractured mudstone and deformed sand layers (Kawamura et al. 2009).

The accretionary prism accumulates methane driven by upward fluid migration, and in a steady-state condition, the BSRs correspond to the base of the gas hydrate stability field (BGHS) (Grevemeyer and Villinger 2001; Yamada et al. 2014), and these are widely distributed in the Nankai subduction zone (Baba and Yamada 2004; Colwell et al. 2004). The forearc basin contains methane hydrates within alternating sediment layers of sand and mud (Suzuki et al. 2009). Fluid containing methane that originates in the décollement migrates upward through faults and intergranular porosity during the accretion process (Yamada et al. 2014) and is evident as cold seeps in the seaward side of the outer wedge (Ashi 1996; Ashi et al. 2002a; Tsuji et al. 2014).

Heat flow has been extensively measured and estimated by BSRs offshore the eastern Kii Peninsula (e.g., Kinoshita et al. 2008; Hamamoto et al. 2011). However, heat flow data are sparse off the western part of the Kii Peninsula. Moreover, several geophysical studies, including seismic and gravity surveys, have suggested the presence of a pluton beneath the Kii Peninsula and its south offshore area (Kodaira et al. 2006; Kimura et al. 2014, 2022; Arnulf et al. 2022). Those studies have suggested that this plutonic rock intruded during the middle Miocene into the upper plate of the island arc crust. However, the relationship between this intrusion and the thermal structure of the Kii Peninsula is still unclear.

Seismic data

The Japan Agency for Marine-Earth Science and Technology (JAMSTEC) acquired two-dimensional multichannel seismic data and high-resolution bathymetric data collected from the central Nankai Trough in 2018 with R/V *Kaimei* (Nakamura et al. 2022). In this study, we used six survey lines from that survey to investigate the relationship between heat flow distribution and active faults (Fig. 1). A tuned airgun array of totaling 173 L with 13.8 MPa (2000 psi) was fired with a shot interval of 50 m, and reflected waveforms were recorded on a towed hydrophone streamer 4.5 km long with a channel interval of 3.125 m. Data were acquired at a sample interval of 2 ms and a record length of 14 s.

Methods

Seismic processing and automated velocity analysis

Before performing automated velocity analysis, several signal enhancement and noise reduction techniques were undertaken (Fig. 2). In this study, we used multi-channel seismic data after preprocessing, including noise reduction, deghosting, designature, debubble, and multiple reflection attenuation (Nakamura et al. 2022). In addition, we applied a bandpass filter with a frequency range of 5–90 Hz to extract the appropriate frequency range of dominant reflection signals. A predictive deconvolution filter was then applied to remove the effects of swell or bubbling. To reduce the computational cost, we decimated shot domain gathers from a 3.125 m to a 6.25 m interval, thus changing the common mid-point (CMP) interval to 3.125 m. After the sorting process, the total number of CMPs was approximately 24,000 for each line.

A high-resolution P-wave velocity structure, determined by velocity analysis, is crucial to accurately map BSR depth and estimate heat flow distributions. We applied automated velocity analysis for this purpose (Fomel et al. 2013), allowing us to estimate seismic velocity from all CMP gathers. Automated velocity picking takes place on calculated semblance panels (Fomel 2009). We first generate a semblance panel of root-mean-square velocity, ranging from 1400 m/s to 2000 m/s with an interval of 20 m/s at every time sample. After estimating root-mean-square velocity by automatically picking semblance peaks (Fomel 2009), the interval velocity was computed based on Dix's equation (Dix 1955). We achieved a high spatial resolution in the resultant velocity structure by estimating seismic velocity from all CMP gathers. Finally, post-stack time migration (post-STM) and depth conversion was applied to all profiles.

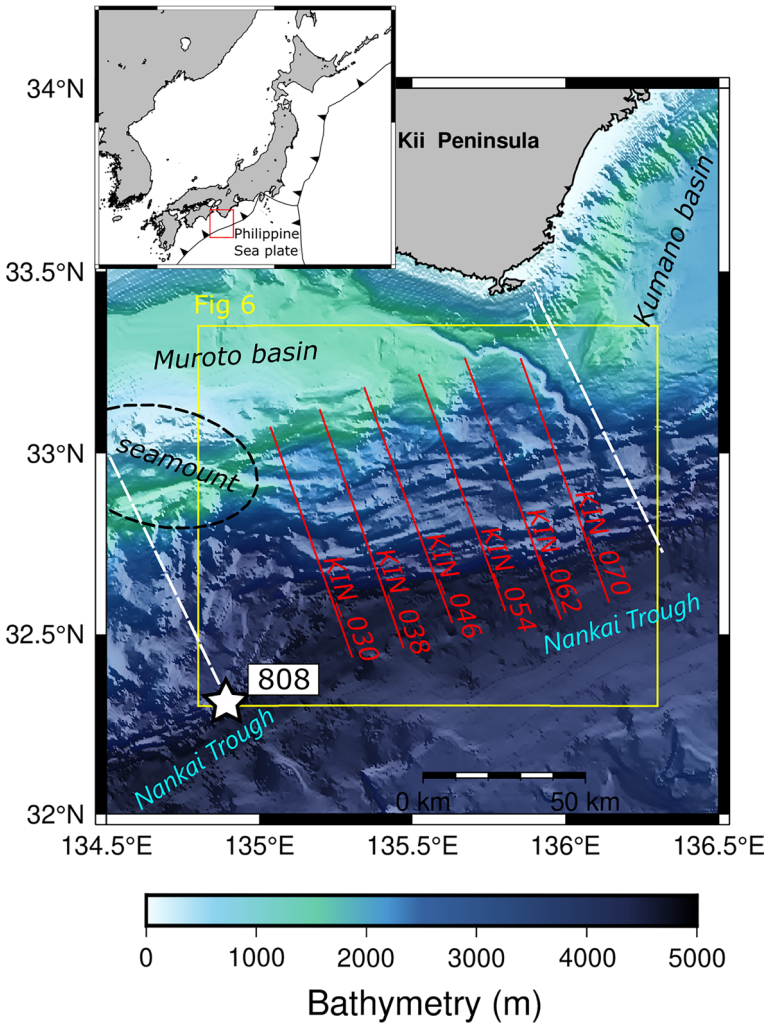

Fig. 1 Bathymetric map of the landward side of the Nankai Trough off the Kii Peninsula. The black triangles along the plate boundaries on the upper panel denote the subduction trend. R/V *Kaimei* KM18-10 seismic survey lines are shown in red. The black dashed region is the location of subducted seamount inferred by Kodaira et al. 2000. White dashed lines are the segment of megathrust rupture along the Nankai Trough (Ando 1975; Cummins et al. 2002). The white star indicates the location of Ocean Drilling Program Sites 808 (Mikada et al. 2002)

BSR picking and heat flow calculation

After the depth conversion of seismic profiles, we picked BSRs manually at every 50 CMP number, which is equivalent to approximately 156 m. The lateral resolution and resolvable thickness of layers on seismic profiles is related to the Fresnel Zone and law of quarter wavelength (e.g., Lindsey 1989; Sheriff 2002). This gives the first Fresnel Zone diameter of 200 m and minimum resolvable thickness of 10 m for the KM18-10 processed seismic data. The picked horizontal interval, which is shorter than the lateral resolution, is reasonable since migration reduces the Fresnel Zone radius.

Since a BSR coincides with the BGHS (Grevemeyer and Villinger 2001) in a static system, the required parameters for heat flow calculations can be inferred from BSR depth. We calculated heat flow based on Fourier's law:

$$Q = -k\frac{T_{\mathrm{BSR}} - T_{\mathrm{Seafloor}}}{Z_{\mathrm{BSR}} - Z_{\mathrm{Seafloor}}}, \tag{1}$$

where Q is heat flow [mW/m^2], k is the bulk thermal conductivity of the sediment between the seafloor and BSR [W/mK], T is temperature [K], and Z is depth [km]. The thermal conductivity can be calculated from P-wave velocity by using an empirical relationship (Duffaut et al. 2018); however, scattering of P-wave velocities may lead to significant errors in thermal conductivity. To remove the effects of scattering, we assumed a thermal conductivity of 1.2 W/mK by averaging the estimated velocity values between the seafloor and the BSRs. Furthermore, we estimated the geothermal gradient from BSR depth by assuming hydrostatic pressure conditions (Ashi and Taira 1993).

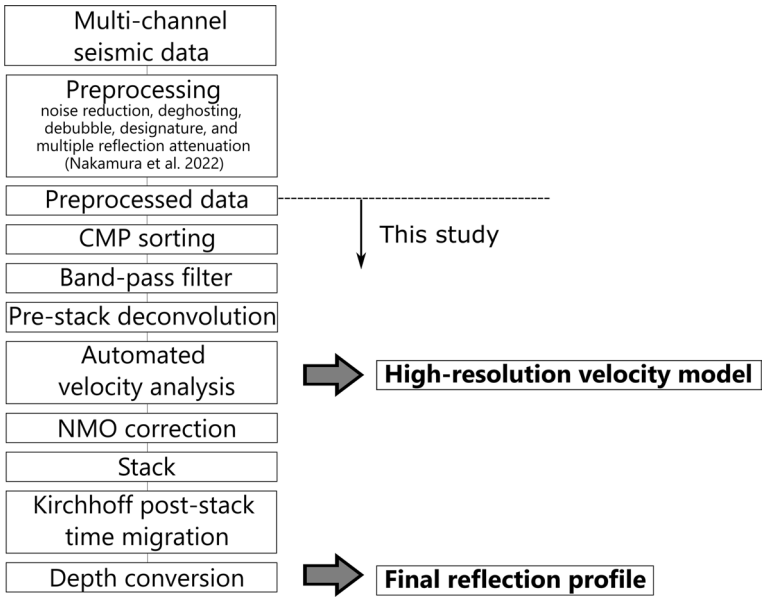

Fig. 2 The flowchart of seismic data processing conducted in this study. Automated velocity analysis was applied on CMP sorted gathers after preprocessing (Nakamura et al. 2022) and additional signal enhancement. Final reflection profile was obtained through depth conversion of the post-stack time migration based on the high-density velocity model

We used the following method to estimate thermal gradients. The hydrostatic pressure at the BSR was estimated from the BSR depth on the seismic profile. We estimated the temperature of the BSR by reference to the methane hydrate phase diagram determined by Hyndman et al. (1992) from laboratory experiments, considering the pure water and pure methane. The seafloor temperature was reported as 2 °C by Integrated Ocean Drilling Program Expeditions 315 and 316 (Harris et al. 2011), and we applied this value to the parameter $T_{seafloor}$. We derived the thermal gradient from the temperature and depth information. Heat flow at each CMP was then estimated by calculating the product of thermal gradient and thermal conductivity (Eq. 1).

Results

P-wave velocity structure

The P-wave velocity structure obtained from our automated velocity analysis revealed detailed geological features in our study area. Since seafloor multiple reflections obscure the deeper part of this structure, we only display P-wave velocity profiles shallower than 1 s in two-way travel time below the seafloor (Fig. 3). This was adequate to identify the BSR, which is located at ~ 0.6 s below the seafloor. By comparing the velocity model and the seismic profile, we determined that the interval velocity range in the sediments containing BSRs was approximately 1800–2300 m/s. The noteworthy feature of velocity analysis is the low-velocity zones (< 1600 m/s), apparent on each velocity profile (Fig. 3, red arrows). The low-velocity zones coincide with major faults (e.g., out-of-sequence thrusts) coring anticline ridges (Fig. 3d) and also observed beneath BSRs (Fig. 3c). Low velocity zones are inferred to reflect the presence of free gas as reported by Chhun et al. (2018) in the Kumano basin and gas charged fluids migrating along faults into the hydrate stability zone (e.g., Korenaga et al. 1997; Tinivella and Accaino 2000).

BSR picking

We can identify the wide distribution of BSRs clearly on the migrated seismic profiles (Fig. 4). Spatial discontinuities of the BSRs are found around the thrust faulting in the accretionary prisms (Fig. 5). BSRs directly under the seafloor where sedimentation or erosion has occurred recently are not parallel to the seafloor or have an edge that diverges from parallel (Fig. 5). Indeed, we observed the double BSR on the seaward part of KIN_054 (Fig. 5b). We picked the lower BSR by considering the erosion effect as we discussed later.

Heat flow

Figure 4 also shows the estimated heat flow and the corresponding seismic depth profiles. The heat flow estimated from the upper part of the accretionary prism to the ITZ ranges from 20 to 100 mW/m^2. From our results, heat flow typically increases in the trenchward direction (Fig. 6b), except at several points inferred as extremely

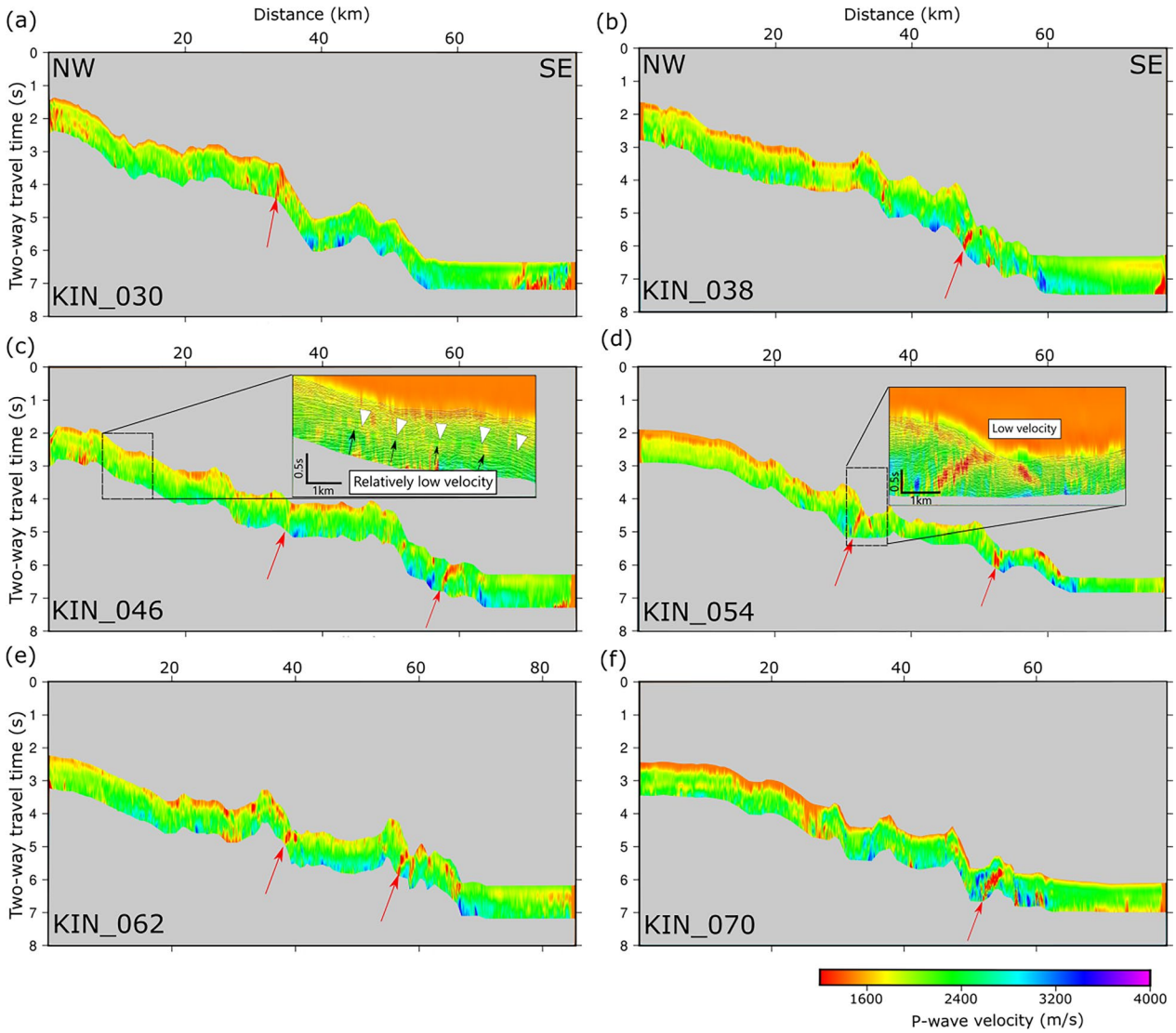

Fig. 3 P-wave velocity structure for all six survey lines in this study. (**a**) Line KIN_030. (**b**) Line KIN_038. (**c**) Line KIN_046. (**d**) Line KIN_54. (**e**) Line KIN_062. (**f**) Line KIN_070. The area with weak reflections is masked in gray. The expanded views on (**c**) and (**d**) show examples of low-velocity zones. The red and black arrows indicate anomalous low-velocity zones corresponding to thrust faults and relatively low-velocity area below BSRs, which may reflect the presence of the free gas, respectively. The white arrowheads indicate BSR positions

high anomalies (e.g., Fig. 4c, d, f). Each seismic profile indicates multiple lateral trends in heat flow as well as extremely high heat flow anomalies as great as 90 mW/m^2 (Figs. 4d, 5a).

The maps of estimated BSR temperatures and heat flow values show a trenchward increase on all six survey lines (Fig. 6a, b). The range of BSR temperatures in our study area is between 17 °C and 25 °C (Fig. 6a), which is consistent with in-situ temperature records determined by long-term borehole monitoring in the Kumano forearc basin (Sugihara et al. 2014). The map in Fig. 6 is limited to the range of 30–60 mW/m^2 to emphasize local heat flow trends (see Additional file 1: Figure S1 for the map showing the full-width color scale of heat flow). Our heat flow distribution (Fig. 6b) generally agrees with previous studies (e.g., Marcaillou et al. 2012; Ohde et al. 2018) except near the eastern end, where our estimate was slightly higher (line KIN_070 in Fig. 6b).

Here, we note the three main sources of uncertainty in our heat flow estimates: (1) seismic velocity, (2) thermal conductivity, and (3) depth error derived from migration processing approaches. Although there are other possible sources of heat flow uncertainties, such

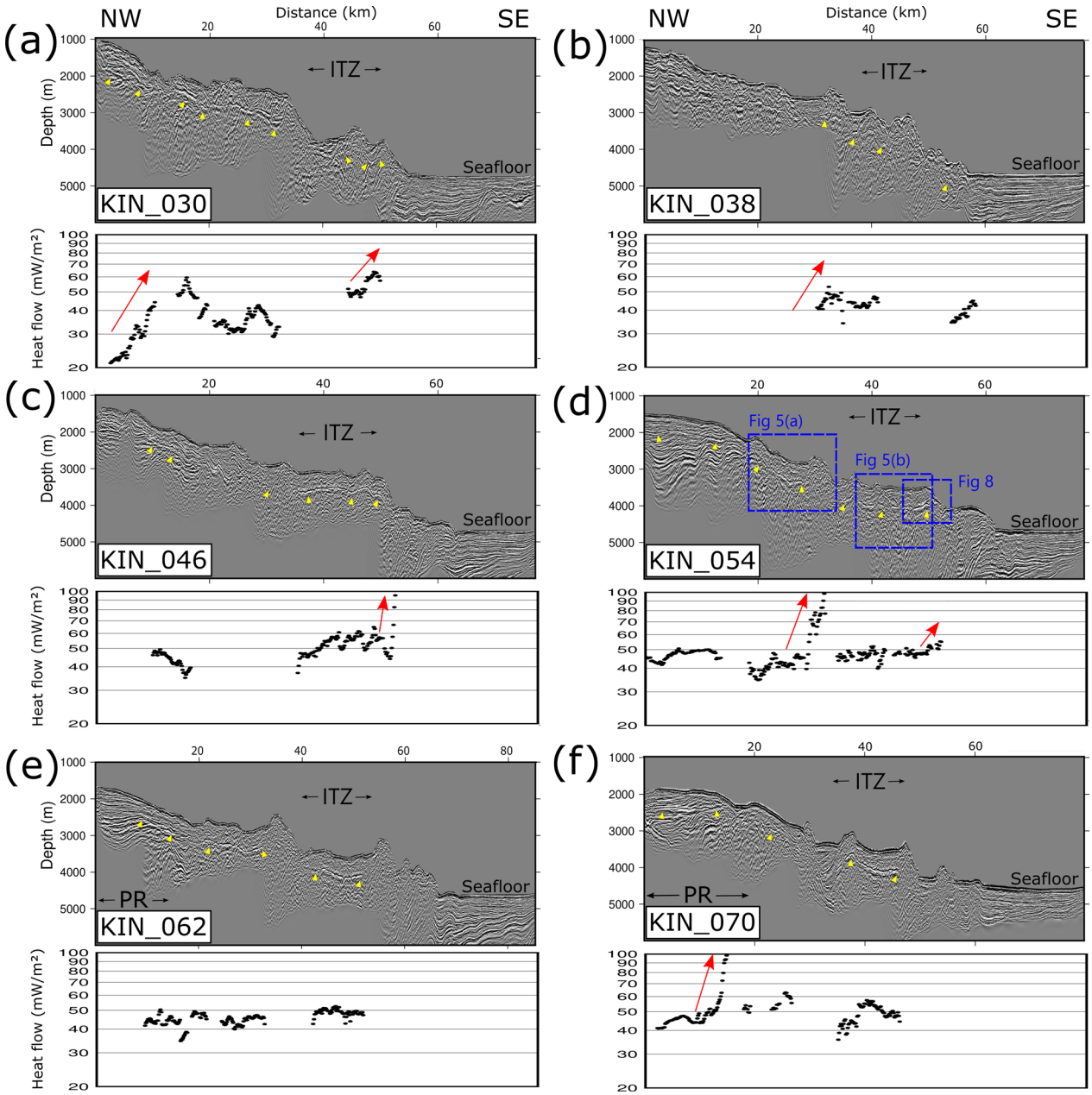

Fig. 4 Seismic depth profile (above) and semilogarithmic heat flow plot (below) for the six survey lines in this study. (**a**) Line KIN_030. (**b**) Line KIN_038. (**c**) Line KIN_046. (**d**) Line KIN_54. (**e**) Line KIN_062. (**f**) Line KIN_070. Blue dashed rectangles on (**f**) correspond to the regions shown in Figs. 5 and 8. The Imbricate Thrust Zone (ITZ) was formed in the middle of the accretionary prisms. The plutonic rock (PR) inferred by Kimura et al. 2022 may be underlain in (**e**) and (**f**). Yellow arrowheads denote the BSRs. Red arrows indicate high heat flow anomalies associated with eroded seafloor

as gas composition, salinity, seafloor temperature, and sedimentation, we did not include these factors because we could not confidently quantify their uncertainty. We hence evaluate several possible sources of uncertainty that could be estimated quantitatively: seismic velocity, assumed thermal conductivity, and picked BSR depth.

Seismic velocity

Seismic velocity was a parameter included in several processing steps (e.g., post-STM, depth conversion, and thermal conductivity estimation). To assess the uncertainty of heat flow derived from seismic velocity, we validated the interval velocity obtained by velocity conversion.

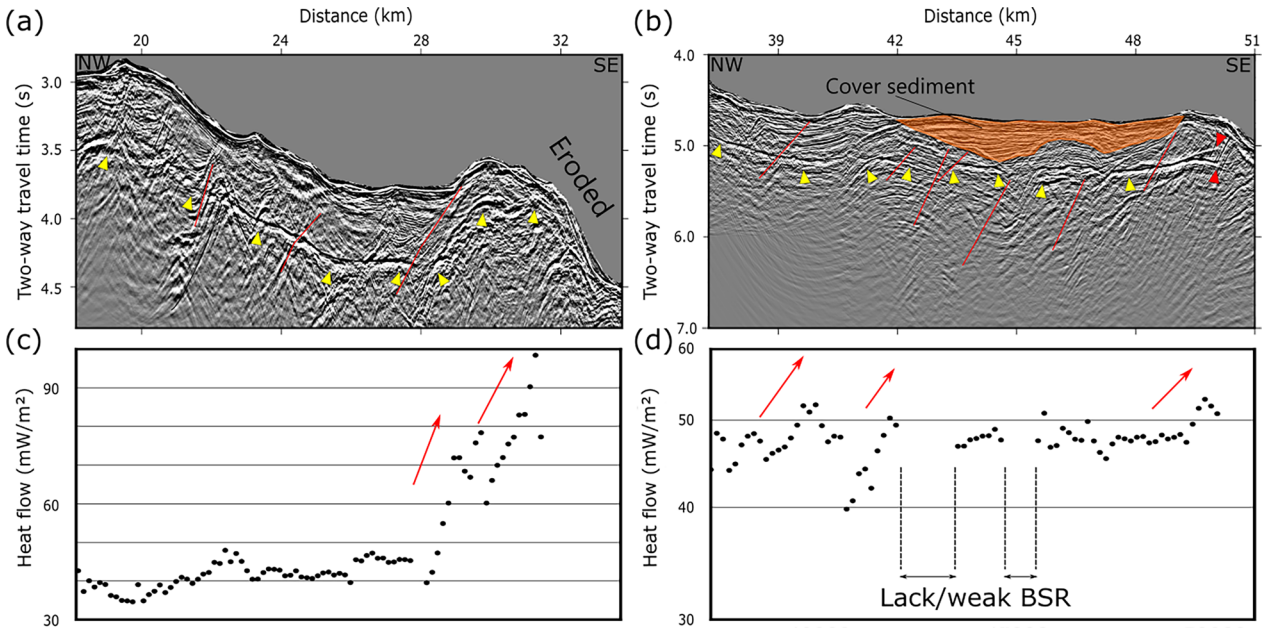

Fig. 5 (**a**), (**b**) Detail of Line KIN_054 seismic profile and (**c**), (**d**) corresponding heat flow plot; location in Fig. 4. Yellow arrowheads denote the BSR. Red arrowheads in (**b**) indicate the relic and migrated BSRs caused by erosion. Red lines and orange translucent zone in (**a**) and (**b**) indicate the interpreted faults and cover sediment, respectively. Red and blue arrows in (**c**) and (**d**) denote local increasing and decreasing trends of heat flow, respectively. Gaps in BSR-derived heat flow data exist in (**d**) because heat flow cannot be estimated where the BSR is absent or weak. Note that the high heat flow anomaly around 50 km in (**b**) corresponds to a feature in the seafloor topography

Since uncertainty in the P-wave velocity within the sequence above the BSR may result in apparent BSR depths that too shallow or too deep (Ohde et al. 2018), we evaluated P-wave velocity within the shallow sequence. We first presumed that the P-wave velocity range in methane-hydrate-bearing sediment was 1800–2300 m/s on the basis of our results of seismic velocity analysis, and then we calculated the BSR depth and the heat flow using velocities of 1800 m/s and 2300 m/s within the corresponding depth in the time domain (two-way-travel time of 0.5 s below the seafloor). Given that we adopted a constant value of thermal conductivity, this velocity variation corresponds directly to a 20% uncertainty in calculated heat flows.

Assumed thermal conductivity

Since we based our constant value of thermal conductivity (1.2 W/mK) on the empirical relationship between P-wave velocity and thermal conductivity (Duffaut et al. 2018), this average value of thermal conductivity differs from the high-resolution record derived from borehole data (Ganguly et al. 2000). To evaluate the resulting uncertainty, we referred to measured thermal conductivity data from Ocean Drilling Program Sites 808 (Fisher 1993) and International Ocean Drilling Program Sites C0002 (Sugihara et al. 2014). Since the measured thermal conductivity range in such sediment was 1.0–1.5 W/mK, the uncertainty in thermal conductivity may be as great as 25% and would lead to a similar uncertainty of heat flow.

Depth error derived from migration processing approaches

Although we performed post-STM in the interest of saving computation costs, seismic profiles obtained from pre-stack time migration (pre-STM) are more accurate than those obtained from post-STM. We evaluated the difference in heat flow derived from the two methods in the shallow sequence above the BSR.

As shown in Fig. 7a and b, we created seismic profiles using post-STM and pre-STM, and then we converted them to the depth domain using the same P-wave velocity model, which is produced by the high-density velocity analysis noted above, to evaluate the error due to the migration processing approach. Finally, we calculated the heat flow in each profile, which is compared in Fig. 7c. Even though the resultant depth profiles agree with the seafloor depth, the BSR depth differed slightly in several parts of the profile (Fig. 7d), corresponding to a difference in heat flow as great as 13%. We concluded that the uncertainty due to the migration processing approach reaches ± 13%.

Although the total uncertainty integrated individual uncertainty is higher than those of similar studies (Ganguly et al. 2000; Townend 1999; Ohde et al. 2018), the

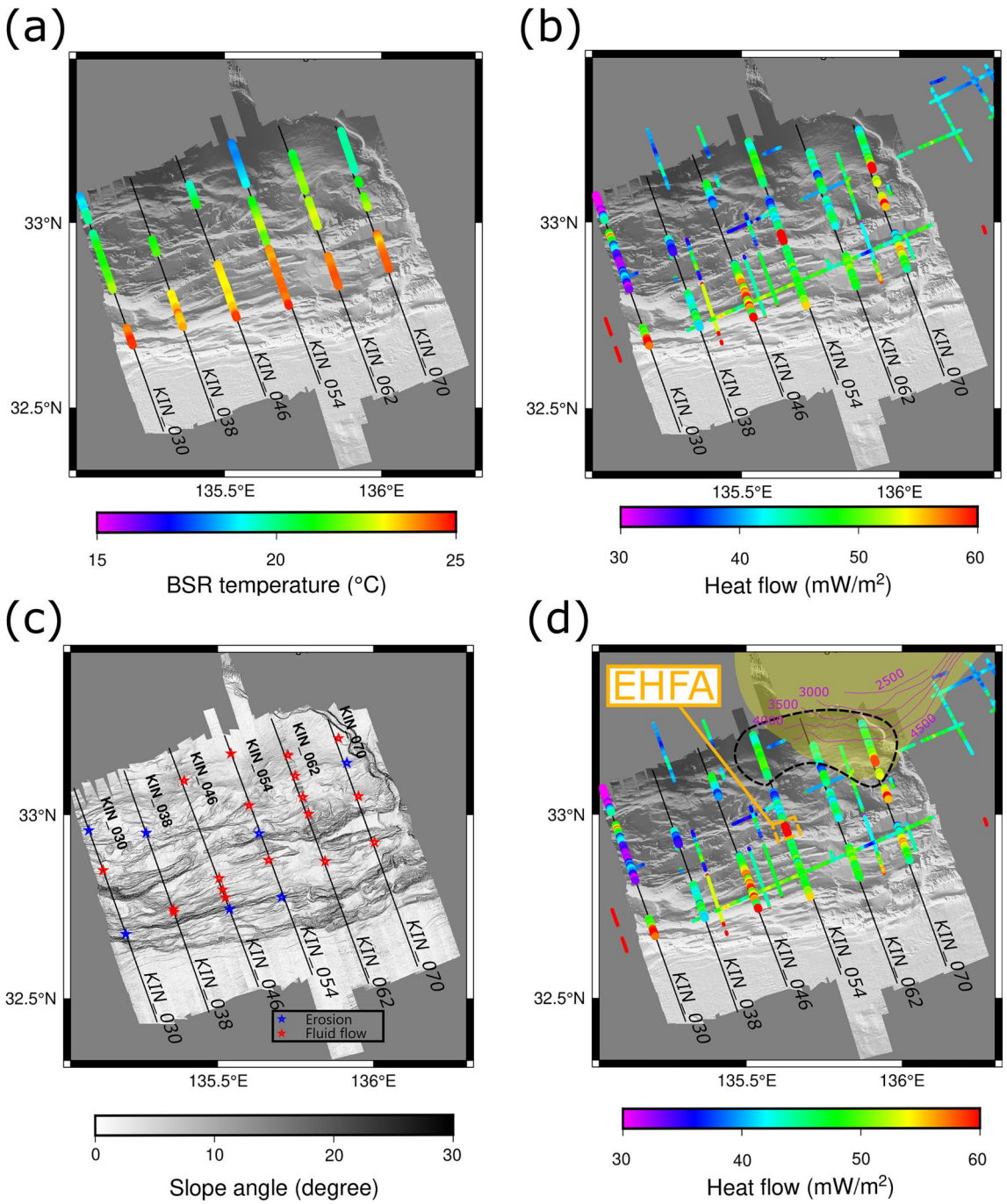

Fig. 6 Distribution of (**a**) BSR temperature and (**b**) heat flow off the Kii Peninsula. Thick and thin lines show our results and the results of Ohde et al. (2018), respectively. Note that the range of the color scale in (**b**) is limited to 30–60 mW/m^2 so as to emphasize heat flow anomalies caused by fluid migration. Higher values are omitted. (**c**) Location of active faults related to erosion or fluid migration, which are inferred from our interpretation of topography heat flow, and seismic profiles. The topographic feature is shown as slope angles derived from high-resolution bathymetry. (**d**) Heat flow in this study area with geological features superimposed. The black dashed circle and yellow dashed region indicate the zone with the anomalous high heat flow and the extremely high heat flow area (EHFA), shown in Fig. 5a, respectively. The yellow translucent area with depth contours indicates the distribution of plutonic rocks, inferred from on-land exposures and apparent beneath an unconformity between the cover sediment and the igneous basement on the seismic profiles (Kimura et al. 2022)

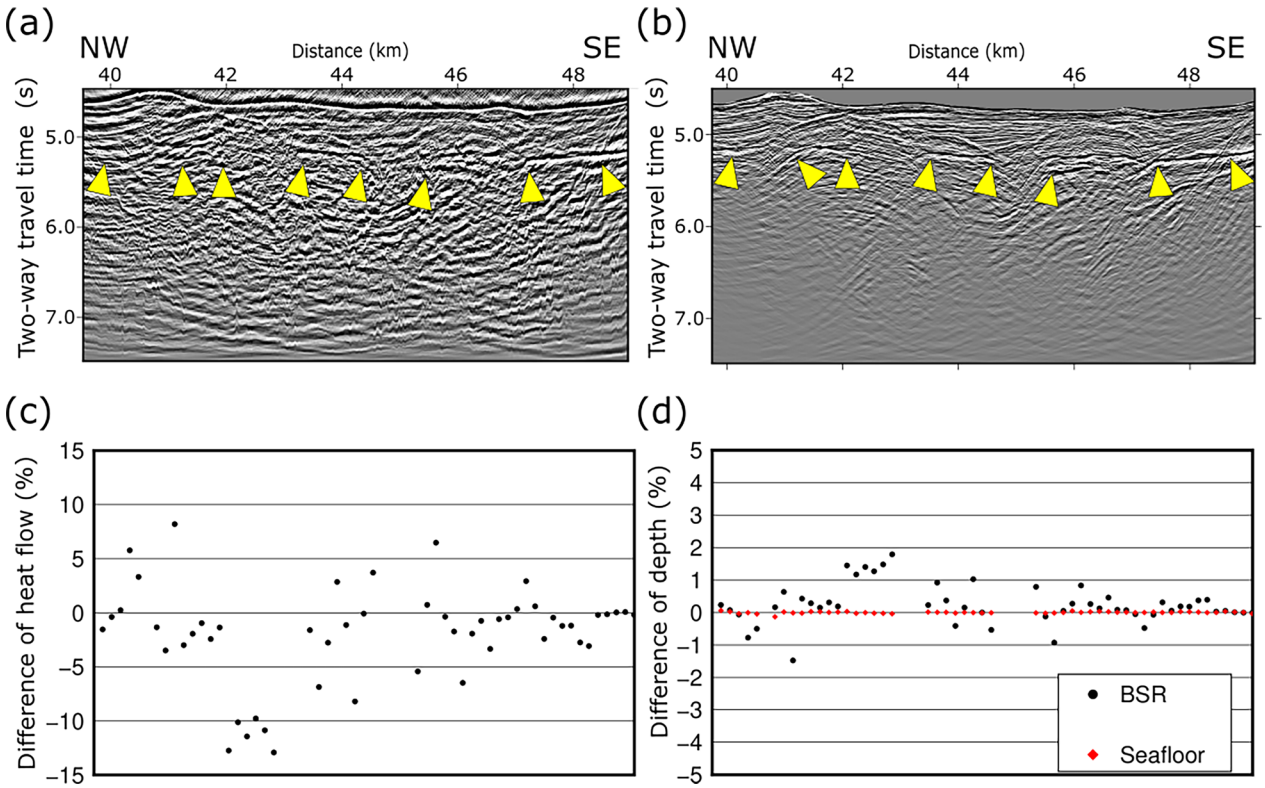

Fig. 7 Extracted seismic profiles obtained by (**a**) pre-STM and (**b**) post-STM. (**c**) The difference in heat flow between (**a**) and (**b**). (**d**) The difference between BSR depth and seafloor depth in profiles obtained by pre-STM (black) and post-STM (red). Note the different vertical scales of (**c**) and (**d**). Yellow arrowheads in (**a**) and (**b**) represent the location of BSRs. The main factors for the uncertainty can be caused by the difference of the BSR depths

effects of some errors cancel and relative errors comparing profile to profile is perhaps less than 10% (Marcaillou et al. 2006).

Discussion

Factors of high heat flow anomalies

Although the map of BSR temperature (Fig. 6a) shows moderate values and few if any apparent anomalies, the map of heat flow (Fig. 6b) shows notable anomalies on each seismic profile. The reasons for these have been discussed in previous studies (e.g., Martin et al. 2004; Yamano et al. 1992; Ohde et al. 2018).

The inferred high heat flow anomalies shown in Figs. 5a and b appear to be associated with seafloor erosion and fluid flow heat advection along active faults (e.g., Martin et al. 2004; Kunath et al. 2021). In Fig. 5a, the BSR in the seaward portion of KIN_054 is not parallel to the seafloor and is likely modified by surface erosion along the seaward flank of the prominent anticline (Fig. 6d). Since the BSR depth is shallow, heat flows in the vicinity of surface erosion have high values. In contrast, in Fig. 5b, the sediment suppresses heat flow variations. On the basis of our results of seismic profile and heat flow estimates, we concluded that the spatial variation of heat flow implies anomalous characteristics in the subsurface. Here, we propose two influencing factors that are consistent with the presence of active faults: erosion and fluid migration.

Erosion

Martin et al. (2004) pointed out that heat flow anomalies derived from BSR can be caused by erosion and sedimentation. Our results indicate extremely high heat flow values, approximately 100 mW/m^2, in the accretionary prism (Fig. 4d). Such anomalies can be caused by erosion and could rival or exceed those caused by fluid flow (Martin et al. 2004) (Fig. 5). Despite our inability to confidently apportion between erosion and fluid flow as causes for the observed heat flow anomalies, at least some erosion-induced heat flow anomaly is expected to exist here because this tectonic setting is known to contain active faulting, which has shown to enhance erosion along the seaward flanks of growing anticline seafloor ridges (Alves et al. 2014).

A general assumption that the BSR marks a stable thermal condition and an equivalence to the BGHS (Grevemeyer and Villinger 2001; Yamada et al. 2014) can be

invalid where erosion or sedimentation has occurred (Martin et al. 2004). Tectonic factors which generate topographic uplift can thus produce non-equilibrium temperature profiles that yield uncertainties in heat flow (Mandal et al. 2014). After a disturbance, the BGHS migrates upward or downward in response to any changes in temperature and pressure conditions. Delisle et al. (1998) reported BSR downward migration due to rapid erosion (slope failure) and upward migration due to rapid sedimentation, resulting in errors in heat flow values of roughly 5%. Kinoshita et al. (2011) have reported that the time for the BSR to re-equilibrate after such a disturbance is ~ 10 kyr in the Nankai accretionary prism. Therefore, the BSR temperature profiles in regions affected by tectonic disturbances might be subject to non-equilibrium conditions that affect the heat flow value.

In addition, several factors (e.g., tectonic uplift and gas sources) can affect the depth of BGHS and thus constrain the BSR positions, including double BSRs (Matsumoto et al. 2004; Zhang et al. 2022). In our study area, we interpret instances of recent BSR downward migrations near sites of erosion (Fig. 8) as well as eroded areas without a corresponding migration and thereby can interpret erosion as the cause of the BSR migration. As mentioned above, BSR migration can take place for several thousands of years to keep thermal equilibrium conditions again. Thus, if the eroded areas without a corresponding migration reflect non-equilibrium conditions, then the extremely high heat flow anomalies observed may be consistent with recent or ongoing fault activity.

Fluid migration

We detected local high heat flow anomalies in the ITZ at locations where erosion cannot be unambiguously identified, and for this reason, we considered that BSR depth may be perturbed by fluid flow causing heat advection (Fig. 5b, d). Fluid flow in the accretionary prism could partially originate in the décollement and rise toward the seafloor into the ITZ, where a BSR forms (Yamano et al. 1992; Baba and Yamada 2004). Our velocity models show low-velocity zones accompanying frontal or out-of-sequence thrusts (Fig. 3). This observation is consistent with fluid flow along major thrust faults (Fig. 9). Moreover, in the region of pronounced heat flow anomalies, thrust faults appear to be exposed at the seafloor, whereas in areas with low heat flows, the faults are blanketed by slope sediments. Since sediment cover is likely to impede or prevent fluid flow (Kobayashi 2002), slope sediments in the ITZ may act to impede fluid flow through the thrust faults. Since our results of heat flow reflect the BSR depth, the area without high heat flow anomalies may indicate an absence of fluid flow along a fault. Although a conclusive determination of the activity status of sediment-covered faults cannot be reliably made based solely on heat flow analysis, the conspicuous absence of cover sediment deformation resulting from fault displacement suggests that the faults in this area could be inactive (Fig. 9) or sedimentation is very rapid.

We classified high heat flow anomalies on the basis of heat flow values, the nearby topography, and the seismic profiles. Where the seafloor appeared to be eroded above faults near a high heat flow anomaly, we assigned it an erosional origin. This type of anomaly also tended to have higher heat flows than anomalies suspected to have been caused by fluid migration. High heat flow anomalies attributed to fluid flow tended to be in the accretionary prism and to be surrounded by low heat flow anomalies, where the presence of slope sediments may inhibit fluid flow.

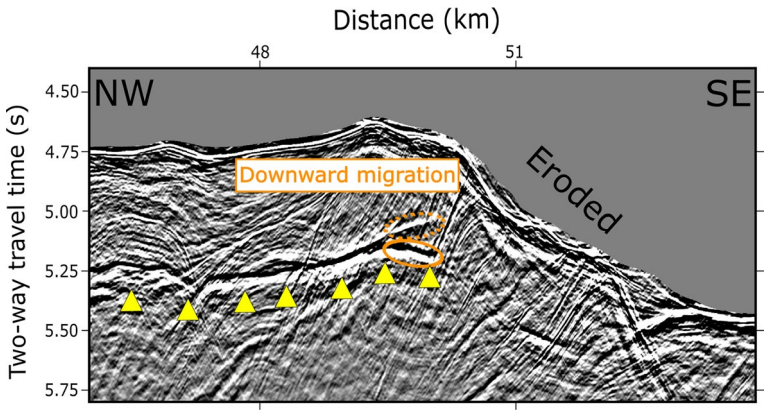

Fig. 8 Detail of the seismic profile of Line KIN_054. Yellow arrowheads indicate the BSR. The orange dashed and solid regions indicate the BSR before and after depth change constrained by thermal conditions, respectively. The edge of the BSR has moved downward at its seaward end in response to plausible surface erosion, though it also could be caused by other factors

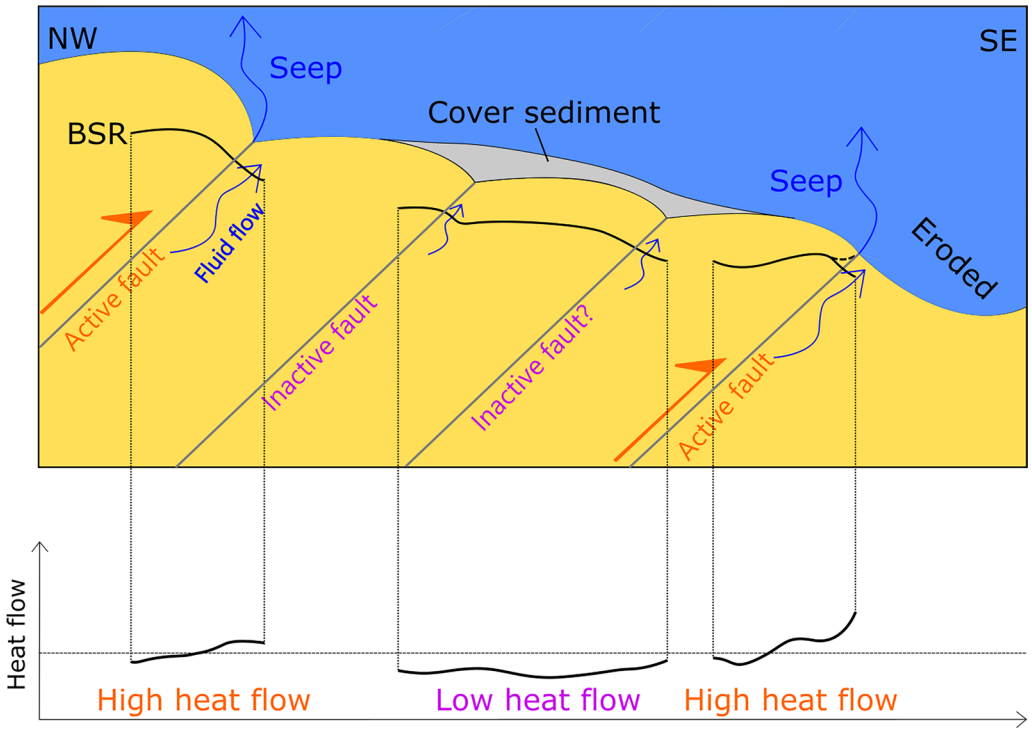

Fig. 9 Schematic image of geological features and heat flow distribution. The orange arrows represent the fault displacement. Where slope sediment covers thrust faults, low heat flow is found. At such sites, the sediment cover might prevent fluid flow (small blue arrows). Areas without cover sediment and with eroded surfaces have high heat flow. Around these areas, fluid flow may reach the seafloor through the active faults (large blue arrows). Near the eroded seafloor, there may be two BSRs: one that represents the pre-erosional pressure and thermal regime (black dashed line at the rightmost part), and another that has since diverged away from the seafloor in response to the post-erosional pressure and thermal regime (black line). Such surface disturbances can also contribute to high heat flow anomalies

Figure 6c plots the locations of active faults based on our joint interpretation of the seismic profiles and heat flow plots. Anomalies attributed to fluid flow are dominant in our study area. In several areas, we cannot estimate the heat flow, nor can we infer or rule out the presence of active faults due to the absence of the BSR, which might be associated with tectonic activities such as surface erosions. Nevertheless, the estimated locations of active faults are consistent with the results of previous studies (e.g., Tsuji et al. 2014).

Landward heat flow trends

Our heat flow distribution shows a general trend of decreasing from ~ 50 mW/m^2 to < 40 mW/m^2 landward (Fig. 6b), which reflects the processes of thickening accretionary wedge sediments and subduction of the Philippine Sea plate. This trend is consistent with previous studies (e.g., Ashi et al. 2002b; Hamamoto et al. 2011; Harris et al. 2013). One noteworthy feature is that the heat flow on Line KIN_030, the westernmost profile, differs from the other survey lines in having some exceptionally low heat flow values. A subducted seamount has been detected beneath the accretionary prism to the west of this profile (e.g., Park et al. 1999; Kodaira et al. 2000; Gulick et al. 2004; Nakamura et al. 2022), which may affect the heat flow profile in two contrasting ways. Spinelli and Harris (2011) have pointed out that the subduction of a seamount would impede fluid flow by closing original pathways and consequently lessen the advective transfer of heat. Likewise, the closing of pathways by the seamount subduction may suppress the migration of heated fluid from greater depth to the shallower part in this area and result in a redistribution of heat that would make the landward part lower heat flow with main contribution of conduction in the accreted sediment. In contrast, other studies have argued that seamount subduction may cause fracturing of the upper plate (e.g., Dominguez et al. 1998; Wang and Bilek 2011), in which case these fractures might act as fluid paths and enhance heat flow. Since our seismic profile did not image pervasive fracturing, we interpret the observed low heat flow on profile KIN_030 to be the result of reduced advective heat transfer.

As mentioned above, heat flow generally decreases landward; nevertheless, our results show a zone of relatively anomalous heat flow (> 40 mW/m^2) in the eastern

part of the study area (Fig. 6b, d). The extent of this trend in our study area seems to correspond with the presence of plutonic rocks beneath the Kii Peninsula, which may extend to the offshore (Kodaira et al. 2006; Kimura et al. 2014, 2022; Arnulf et al. 2022). Since the thermal conductivity of plutonic rocks is generally higher than that of sedimentary rocks (Clauser and Huenges 1995) and the regional heat flow is derived from the subducting Philippine Sea plate beneath the onshore and offshore portions of the Kii Peninsula (e.g., Ji et al. 2016), the thermal structure in this region can be constrained by the existence of the plutonic rock. Therefore, the higher thermal conductivity of the plutonic rock may contribute to the high heat flow trend observed in the landward side in the eastern part. The Kii Peninsula contains hot springs with high temperatures, high geothermal gradients, and heat flow anomalies even though this area is not a volcanic region (Furukawa et al. 1998; Yano 1999; Tanaka et al. 2004). These geothermal anomalies may be associated with extensional faults and vertical dykes with N–S strikes (Umeda et al. 2006). Even though there may be still uncertainty of the heat flow profile in our study area, we concluded that the presence of the plutonic rock is contributing to high heat flow trend in our study area.

Conclusions

We conducted seismic processing with automated velocity analysis of parallel seismic profiles acquired during the 2018 R/V *Kaimei* voyage (KM18-10) offshore the Kii Peninsula. Using high-resolution P-wave velocity information, we mapped the distribution of the BSR in the study area. Velocities in the methane hydrate–bearing sediments above the BSR ranged from 1800 to 2300 m/s and allowed us to outline low-velocity zones along the major thrust faults that suggest the presence of advective fluid flow. Heat flow, calculated from the BSR depth, ranged from 20 to 100 mW/m^2, although this range includes uncertainties due to seismic velocity, migration processing approach, and thermal conductivity. Our heat flow distribution map shows high and low anomalies, which can be attributed to seafloor erosion or fluid flow.

High heat flow anomalies due to erosion, which can be confirmed by seismic profiles or bathymetric mapping, can exceed those due to fluid flow. These anomalies can serve as evidence of recent tectonic activity that confirms the existence of active faults. Low heat flow anomalies, detected beneath areas of thick cover sediment on our seismic profiles, are interpreted as the consequence of rapid sedimentation. Areas of high heat flow neighboring these low anomalies are usually not covered by slope sediments and are interpreted as the result of heat advection by fluid flow through thrust faults that reach the seafloor. Since active faults can offer highly permeable fluid paths, active faults may be associated with high heat flow anomalies caused by fluid flow. We also found evidence that parts of the BSR in the study area may represent conditions out of thermal equilibrium.

We noted a trend toward higher heat flow on the landward part of our study area close to the Kii Peninsula. We interpret this higher heat flow anomaly results from the thermal structure of plutonic rocks beneath the Kii Peninsula, which may extend offshore.

Abbreviations

BSR	Bottom-simulating reflector
BGHS	Base of gas hydrate stability
CMP	Common mid-point
Post-STM	Post-stack time migration
ITZ	Imbricate thrust zone
Pre-STM	Pre-stack time migration

Supplementary Information

The online version contains supplementary material available at https://doi.org/10.1186/s40623-023-01890-9.

Additional file 1: Figure S1. Distribution of heat flow off the Kii Peninsula with a wider color scale than Figure 6 (b) and (d).

Acknowledgements

We thank the Japan Agency for Marine-Earth Science Technology for providing seismic data and high-resolution bathymetric data. Seismic processing was conducted by open-source software Madagascar (Fomel et al. 2013) and SU (Seismic Un*x) (Stockwell 1999) on the ITO supercomputer system at the Research Institute for Information Technology, Kyushu University. The figures other than Figures 2 and 9 were prepared with GMT (Generic Mapping Tools) (Wessel and Smith 1991). We are grateful to A. Kioka for meaningful discussions about seismic processing and heat flow calculations. We also thank A. Kioka and J. Ashi for providing BSR-derived heat flow data estimated by Ohde et al. (2018). We thank three anonymous reviewers and the associate editor for providing insightful comments that improved the manuscript.

Author contributions

ST performed the seismic processing and calculated heat flows. TT and KM supervised the seismic processing. ST interpreted the results and wrote the manuscript in discussion with TT, KS, YN, SK, and GF. All the authors read and approved the manuscript. TT conceived this study and supervised ST.

Funding

This study was supported by JSPS Kakenhi Grant Number JP20H01997 and JP21H05202.

Availability of data and materials

The seismic datasets used in this study are available at the JAMSTEC seismic survey database, https://doi.org/10.17596/0002069. The other datasets used and/or analyzed during the current study are available from the corresponding author on reasonable request.

Declarations

Ethics approval and consent to participate

Not applicable.

Consent for publication

Not applicable.

Competing interests

The authors declare that they have no competing interests.

Author details
[1]Department of Earth Resources Engineering, Kyushu University, 744 Motooka Nishi-Ku, Fukuoka 819-0395, Japan. [2]School of Engineering, The University of Tokyo, 7-3-1 Hongo, Bunkyo-Ku, Tokyo 113-8656, Japan. [3]Japan Agency for Marine-Earth Science and Technology (JAMSTEC), 3173-25 Showa-Machi, Kanazawa-Ku, Yokohama 236-0001, Japan.

Received: 14 October 2022 Accepted: 26 August 2023
Published online: 25 September 2023

References

Alves TM, Strasser M, Moore G (2014) Erosional features as indicators of thrust fault activity (Nankai Trough, Japan). Mar Geol 356:5–18. https://doi.org/10.1016/j.margeo.2013.07.011

Ando M (1975) Source mechanisms and tectonic significance of historical earthquakes along the Nankai Trough, Japan. Tectonophysics 27(2):119–140. https://doi.org/10.1016/0040-1951(75)90102-X

Arnulf AF, Bassett D, Harding AJ, Kodaira S, Nakanishi A, Moore G (2022) Upper-plate controls on subduction zone geometry, hydration and earthquake behaviour. Nat Geosci 15(2):143–148

Ashi J (1996) Distribution of cold seepage at the Ryuyo Canyon off Tokai: the 1995 KAIKO-Tokai "Shinkai 2000" Dives. JAMSTEC J Deep-Sea Res 12:160–166

Ashi J, Taira A (1993) Thermal structure of the Nankai accretionary prism as inferred from the distribution of gas hydrate BSRs. Special Paper Geol Soc Am 273(4):137–149. https://doi.org/10.1130/SPE273-p137

Ashi, J, Kuramoto S, Morita S, Tsunogai U, Goto S, Kojima S, Okamoto T, Ishimura T, Ijiri A, Toki T, Kudo S, Asai S, Utsumi M (2002a) Structure and cold seep of the Nankai accretionary prism off Kumano—Outline of the off Kumano survey during YK01-04 Leg 2 Cruise. JAMSTEC J Deep Sea Res, 20

Ashi J, Tokuyama H, Taira A (2002b) Distribution of methane hydrate BSRs and its implication for the prism growth in the Nankai Trough. Mar Geol 187(1–2):177–191. https://doi.org/10.1016/S0025-3227(02)00265-7

Baba K, Yamada Y (2004) BSRs and associated reflections as an indicator of gas hydrate and free gas accumulation: an example of accretionary prism and forearc basin system along the Nankai Trough, off central Japan. Resour Geol 54(1):11–24. https://doi.org/10.1111/j.1751-3928.2004.tb00183.x

Chhun C, Kioka A, Jia J, Tsuji T (2018) Characterization of hydrate and gas reservoirs in plate convergent margin by applying rock physics to high-resolution seismic velocity model. Mar Pet Geol 92:719–732. https://doi.org/10.1016/j.marpetgeo.2017.12.002

Christoffel DA, Calhaem IM (1969) A geothermal heat flow probe for in situ measurement of both temperature gradient and thermal conductivity. J Phys E: Sci Instrum 2(6):457

Clauser C, Huenges E (1995) Thermal conductivity of rocks and minerals. Rock physics and phase relations: a handbook of physical constants, 3: 105–126.

Colwell F, Matsumoto R, Reed D (2004) A review of the gas hydrates, geology, and biology of the Nankai Trough. Chem Geol 205(3–4):391–404. https://doi.org/10.1016/j.chemgeo.2003.12.023

Cummins PR, Baba T, Kodaira S, Kaneda Y (2002) The 1946 Nankai earthquake and segmentation of the Nankai Trough. Phys Earth Planet Inter 132(1–3):75–87. https://doi.org/10.1016/S0031-9201(02)00045-6

Davis EE, Hyndman RD, Villinger H (1990) Rates of fluid expulsion across the Northern Cascadia Accretionary Prism: constraints from new heat row and multichannel seismic reflection data. J Geophys Res Solid Earth 95(B6):8869–8889. https://doi.org/10.1029/JB095iB06p08869

Delisle G, Beiersdorf H, Neben S, Steinmann D (1998) The geothermal field of the North Sulawesi accretionary wedge and a model on BSR migration in unstable depositional environments. Geol Soc Lond Special Publ 137(1):267–274. https://doi.org/10.1144/GSL.SP.1998.137.01.21

Dix CH (1955) Seismic velocities from surface measurements. Geophysics 20:68–86. https://doi.org/10.1190/1.1438126

Dominguez S, Lallemand SE, Malavieille J, von Huene R (1998) Upper plate deformation associated with seamount subduction. Tectonophysics 293(3–4):207–224. https://doi.org/10.1016/S0040-1951(98)00086-9

Duffaut K, Hokstad K, Kyrkjeb R, Wiik T (2018) A simple relationship between thermal conductivity and seismic interval velocity. Lead Edge 37(5):381–385. https://doi.org/10.1190/tle37050381.1

Eng C, Tsuji T (2019) Influence of faults and slumping on hydrocarbon migration inferred from 3D seismic attributes: Sanriku-Oki forearc basin, northeast Japan. Mar Pet Geol 99:175–189. https://doi.org/10.1016/j.marpetgeo.2018.10.013

Fisher AT (1993) Data report: Corrected thermal conductivity data, Leg 131. Proceedings of the Ocean Drilling Program, Scientific Results, College Station, Texas, 131: 451–456

Fomel S (2009) Velocity analysis using AB semblance. Geophys Prospect 57(3):311–321. https://doi.org/10.1111/j.1365-2478.2008.00741.x

Fomel S, Sava P, Vlad I, Liu Y, Bashkardin V (2013) Madagascar: open-source software project for multidimensional data analysis and reproducible computational experiments. J Open Res Softw. https://doi.org/10.5334/jors.ag

Furukawa Y, Shinjoe H, Nishimura S (1998) Heat flow in the southwest Japan arc and its implication for thermal processes under arcs. Geophys Res Lett 25(7):1087–1090. https://doi.org/10.1029/98GL00545

Ganguly N, Spence GD, Chapman NR, Hyndman RD (2000) Heat flow variations from bottom simulating reflectors on the Cascadia margin. Mar Geol 164(1–2):53–68. https://doi.org/10.1016/S0025-3227(99)00126-7

Grevemeyer I, Villinger H (2001) Gas hydrate stability and the assessment of heat flow through continental margins. Geophys J Int 145(3):647–660. https://doi.org/10.1046/j.0956-540x.2001.01404.x

Gulick SPS, Bangs NLB, Shipley TH, Nakamura Y, Moore GF, Kuramoto S (2004) Three-dimensional architecture of the Nankai accretionary prism's imbricate thrust zone off Cape Muroto, Japan: Prism reconstruction via en echelon thrust propagation. J Geophys Res Solid Earth. https://doi.org/10.1029/2003JB002654

Hamamoto H, Yamano M, Goto S, Kinoshita M, Fujino K, Wang K (2011) Heat flow distribution and thermal structure of the Nankai subduction zone off the Kii Peninsula. Geochem Geophys Geosyst. https://doi.org/10.1029/2011GC003623

Harris RN, Schmidt-Schierhorn F, Spinelli G (2011) Heat flow along the NanTroSEIZE transect: Results from IODP Expeditions 315 and 316 offshore the Kii Peninsula, Japan. Geochem Geophys Geosyst. https://doi.org/10.1029/2011GC003593

Harris R, Yamano M, Kinoshita M, Spinelli G, Hamamoto H, Ashi J (2013) A synthesis of heat flow determinations and thermal modeling along the Nankai Trough, Japan. J Geophys Res Solid Earth 118(6):2687–2702. https://doi.org/10.1002/jgrb.50230

Honda R, Kono Y (2005) Buried large block revealed by gravity anomalies in the Tonankai and Nankai earthquakes regions, southwestern Japan. Earth Planets Space 57(1):e1–e4. https://doi.org/10.1186/BF03351799

Hori T (2006) Mechanisms of separation of rupture area and variation in time interval and size of great earthquakes along the Nankai Trough, southwest Japan. Earth Simulator 5:8–19

Hyndman RD, Spence GD (1992) A seismic study of methane hydrate marine bottom simulating reflectors. J Geophys Res Solid Earth 97(B5):6683–6698. https://doi.org/10.1029/92JB00234

Hyndman RD, Foucher JP, Yamano M, Fisher A et al (1992) Deep sea bottom-simulating-reflectors: calibration of the base of the hydrate stability field as used for heat flow estimates. Earth Planet Sci Lett 109:289–301. https://doi.org/10.1016/0012-821X(92)90093-B

Ji Y, Yoshioka S, Matsumoto T (2016) Three-dimensional numerical modeling of temperature and mantle flow fields associated with subduction of the Philippine Sea plate, southwest Japan. J Geophys Res Sol Ear 121:4458–4482. https://doi.org/10.1002/2016JB012912

Kasaya T, Goto TN, Mikada H, Baba K, Suyehiro K, Utada H (2005) Resistivity image of the Philippine Sea Plate around the 1944 Tonankai earthquake zone deduced by Marine and Land MT surveys. Earth Planets Space 57(3):209–213. https://doi.org/10.1186/BF03351817

Kawamura K, Ogawa Y, Anma R, Yokoyama S, Kawakami S, Dilek Y, Moore GF, Hirano S, Yamaguchi A, Sasaki T (2009) Structural architecture and active deformation of the Nankai Accretionary Prism, Japan: submersible survey results from the Tenryu Submarine CanyonOngoing formation of the Nankai accretionary prism. GSA Bull 121(11–12):1629–1646. https://doi.org/10.1130/B26219.1

Kimura G, Hashimoto Y, Kitamura Y, Yamaguchi A, Koge H (2014) Middle Miocene swift migration of the TTT triple junction and rapid crustal growth

in southwest Japan: a review. Tectonics 33(7):1219–1238. https://doi.org/10.1002/2014TC003531
Kimura G, Nakamura Y, Shiraishi K, Fujie G, Kodaira S, Tsuji T, Yamaguchi A (2022) Nankai Forearc structural and seismogenic segmentation caused by a magmatic intrusion off the Kii Peninsula. Geochem Geophys Geosyst. https://doi.org/10.1029/2022GC010331
Kinoshita M, Kanamatsu T, Kawamura K, Shibata T, Hamamoto H, Fujino K (2008) Heat flow distribution on the floor of Nankai Trough off Kumano and implications for the geothermal regime of subducting sediments. JAMSTEC Report Res Dev 8:13–28. https://doi.org/10.5918/jamstecr.8.13
Kinoshita M, Moore GF, Kido YN (2011) Heat flow estimated from BSR and IODP borehole data: implication of recent uplift and erosion of the imbricate thrust zone in the Nankai Trough off Kumano. Geochem Geophys Geosyst. https://doi.org/10.1029/2011GC003609
Kobayashi K (2002) Tectonic significance of the cold seepage zones in the eastern Nankai accretionary wedge–an outcome of the 15 years' KAIKO projects. Mar Geol 187(1–2):3–30. https://doi.org/10.1016/S0025-3227(02)00242-6
Kodaira S, Takahashi N, Nakanishi A, Miura S, Kaneda Y (2000) Subducted seamount imaged in the rupture zone of the 1946 Nankaido earthquake. Science (new York NY) 289(5476):104–106. https://doi.org/10.1126/science.289.5476.104
Kodaira S, Hori T, Ito A, Miura S, Fujie G, Park JO, Baba T, Sakaguchi H, Kaneda Y (2006) A cause of rupture segmentation and synchronization in the Nankai trough revealed by seismic imaging and numerical simulation. J Geophys Res Solid Earth. https://doi.org/10.1029/2005JB004030
Kodaira S, Sato T, Takahashi N, Miura S, Tamura Y, Tatsumi Y, Kaneda Y (2007) New seismological constraints on growth of continental crust in the Izu-Bonin intra-oceanic arc. Geology 35(11):1031–1034. https://doi.org/10.1130/G23901A.1
Korenaga J, Holbrook WS, Singh SC, Minshull TA (1997) Natural gas hydrates on the southeast US margin: constraints from full waveform and travel time inversions of wide-angle seismic data. J Geophys Res Solid Earth 102(B7):15345–15365. https://doi.org/10.1029/97JB00725
Kret K, Tsuji T, Chhun C, Takano O (2020) Distributions of gas hydrate and free gas accumulations associated with upward fluid flow in the Sanriku-Oki forearc basin, northeast Japan. Marine Petroleum Geol 116:104305. https://doi.org/10.1016/j.marpetgeo.2020.104305
Kunath P, Chi WC, Berndt C, Liu CS (2021) A rapid numerical method to constrain 2D focused fluid flow rates along convergent margins using dense BSR-based temperature field data. J Geophys Res Solid Earth 126(7):e2021JB021668. https://doi.org/10.1029/2021JB021668
Lindsey JP (1989) The Fresnel zone and its interpetive significance. Lead Edge 8(10):33–39. https://doi.org/10.1190/1.1439575
Mandal R, Dewangan P, Ramprasad T, Kumar BJP, Vishwanath K (2014) Effect of thermal non-equilibrium, seafloor topography and fluid advection on BSR-derived geothermal gradient. Mar Pet Geol 58:368–381. https://doi.org/10.1016/j.marpetgeo.2014.04.002
Marcaillou B, Spence G, Collot JY, Wang K (2006) Thermal regime from bottom simulating reflectors along the north Ecuador–south Colombia margin: relation to margin segmentation and great subduction earthquakes. J Geophys Res Solid Earth. https://doi.org/10.1029/2005JB004239
Marcaillou B, Henry P, Kinoshita M, Kanamatsu T, Screaton E, Daigle H, Yamano M (2012) Seismogenic zone temperatures and heat-flow anomalies in the To-nankai margin segment based on temperature data from IODP expedition 333 and thermal model. Earth Planet Sci Lett 349:171–185. https://doi.org/10.1016/j.epsl.2012.06.048
Markl RG, Bryan GM, Ewing JI (1970) Structure of the Blake-Bahama outer ridge. J Geophys Res 75(24):4539–4555. https://doi.org/10.1029/JC075i024p04539
Martin V, Henry P, Nouze H, Noble M, Ashi J, Pascal G (2004) Erosion and sedimentation as processes controlling the BSR-derived heat flow on the Eastern Nankai margin. Earth Planet Sci Lett 222(1):131–144. https://doi.org/10.1016/j.epsl.2004.02.020
Matsumoto R, Tomaru H, Lu H (2004) Detection and evaluation of gas hydrates in the eastern Nankai Trough by geochemical and geophysical methods. Resour Geol 54(1):53–67. https://doi.org/10.1111/j.1751-3928.2004.tb00187.x
Mikada H, Becker K, Moore JC, Klaus A et al (2002) In: Proceedings of the ocean drilling program initial reports volume 196. Ocean Drilling Program, College
Mukumoto K, Tsuji T, Hendriyana A (2019) Large gas reservoir along the rift axis of a continental back-arc basin revealed by automated seismic velocity analysis in the Okinawa trough. Geophys Res Lett. https://doi.org/10.1029/2019GL083065
Nakamura Y, Shiraishi K, Fujie G, Kodaira S, Kimura G, Kaiho Y, No T, Miura S (2022) Structural anomaly at the boundary between strong and weak plate coupling in the Central-western Nankai Trough. Geophys Res Lett 49(10):e2022GL098180. https://doi.org/10.1029/2022GL098180
Ohde A, Otsuka H, Kioka A, Ashi J (2018) Distribution and depth of bottom-simulating reflectors in the Nankai subduction margin. Earth Planets Space 70(1):1–20. https://doi.org/10.1186/s40623-018-0833-5
Park JO, Tsuru T, Kaneda Y, Kono Y, Kodaira S, Takahashi N, Kinoshita H (1999) A subducting seamount beneath the Nankai accretionary prism off Shikoku, southwestern Japan. Geophys Res Lett 26(7):931–934. https://doi.org/10.1029/1999GL900134
Seno T, Stein S, Gripp AE (1993) A model for the motion of the Philippine Sea plate consistent with NUVEL-1 and geological data. J Geophys Res Solid Earth 98(B10):17941–17948. https://doi.org/10.1029/93JB00782
Sheriff RE (2002) Encyclopedic dictionary of applied geophysics. Society of exploration geophysicists
Spinelli GA, Harris RN (2011) Thermal effects of hydrothermal circulation and seamount subduction: temperatures in the Nankai Trough Seismogenic Zone Experiment transect, Japan. Geochem Geophys Geosyst. https://doi.org/10.1029/2011GC003727
Stockwell JW Jr (1999) The CWP/SU: seismic Un∗ x package. Comput Geosci 25(4):415–419. https://doi.org/10.1016/S0098-3004(98)00145-9
Sugihara T, Kinoshita M, Araki E, Kimura T, Kyo M, Namba Y, Thu MK (2014) Re-evaluation of temperature at the updip limit of locked portion of Nankai megasplay inferred from IODP Site C0002 temperature observatory. Earth Planets Space 66(1):1–14. https://doi.org/10.1186/1880-5981-66-107
Suzuki K, Ebinuma T, Narita H (2009) Features of Methane Hydrate-bearing Sandy-sediments of the Forearc Basin along the Nankai Trough: effect on Methane Hydrate-Accumulating Mechanism in Turbidite. J Geogr 118(5):899–912. https://doi.org/10.5026/jgeography.118.899
Tanaka A, Yamano M, Yano Y, Sasada M (2004) Geothermal gradient and heat flow data in and around Japan (I): appraisal of heat flow from geothermal gradient data. Earth Planets Space 56(12):1191–1194. https://doi.org/10.1186/BF03353339
Tinivella U, Accaino F (2000) Compressional velocity structure and Poisson's ratio in marine sediments with gas hydrate and free gas by inversion of reflected and refracted seismic data (South Shetland Islands, Antarctica). Mar Geol 164(1–2):13–27. https://doi.org/10.1016/S0025-3227(99)00123-1
Tsuji T, Ashi J, Ikeda Y (2014) Strike-slip motion of a mega-splay fault system in the Nankai oblique subduction zone. Earth Planets Space 66(1):1–14. https://doi.org/10.1186/1880-5981-66-120
Umeda K, Ogawa Y, Asamori K, Oikawa T (2006) Aqueous fluids derived from a subducting slab: Observed high 3He emanation and conductive anomaly in a non-volcanic region, Kii Peninsula southwest Japan. J Volcanol Geoth Res 149(1–2):47–61
Vanneste M, De Batist M, Golmshtok A, Kremlev A, Versteeg W (2001) Multi-frequency seismic study of gas hydrate-bearing sediments in Lake Baikal, Siberia. Marine Geol 172(1–2):1–21. https://doi.org/10.1016/S0025-3227(00)00117-1
Wang K, Bilek SL (2011) Do subducting seamounts generate or stop large earthquakes? Geology 39(9):819–822. https://doi.org/10.1130/G31856.1
Wessel P, Smith WH (1991) Free software helps map and display data. EOS Trans Am Geophys Union 72(41):441–446. https://doi.org/10.1029/90EO00319
Yamada Y, Baba K, Miyakawa A, Matsuoka T (2014) Granular experiments of thrust wedges: insights relevant to methane hydrate exploration at the Nankai accretionary prism. Mar Pet Geol 51:34–48. https://doi.org/10.1016/j.marpetgeo.2013.11.008
Yamano M, Uyeda S, Aoki Y, Shipley TH (1982) Estimates of heat flow derived from gas hydrates. Geology 10(7):339–343. https://doi.org/10.1130/0091-7613(1982)10%3C339:EOHFDF%3E2.0.CO;2
Yamano M, Foucher JP, Kinoshita M, Fisher A, Hyndman RD, Leg ODP, Party SS (1992) Heat flow and fluid flow regime in the western Nankai accretionary prism. Earth Planet Sci Lett 109(3–4):451–462. https://doi.org/10.1016/0012-821X(92)90105-5

Yano Y (1999) Geothermal gradient map of Japan 1: 3000000. Geological Survey of Japan
Zhang W, Liang J, Qiu H, Deng W, Meng M, He Y, Wang F (2022) Double bottom simulating reflectors and tentative interpretation with implications for the dynamic accumulation of gas hydrates in the northern slope of the Qiongdongnan Basin, South China Sea. J Asian Earth Sci 229:105151. https://doi.org/10.1016/j.jseaes.2022.105151

Publisher's Note